

ESA Climate Change Initiative (CCI+)

Essential Climate Variable (ECV)

Antarctic_Ice_Sheet_cci+ (AIS_cci+)

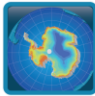
End-to-end Uncertainty Budget (E3UB)

Prime & Science Lead: Andrew Shepherd
University of Leeds, Leeds, United Kingdom
a.shepherd@leeds.ac.uk

Technical Officer: Marcus Engdahl
ESA ESRIIN, Frascati, Italy
Marcus.Engdahl@esa.int

Consortium:

- DTU Microwaves and Remote Sensing Group (DTU-N)
- DTU Geodynamics Group (DTU-S)
- ENVironmental Earth Observation GmbH (ENVEO)
- Deutsches Zentrum für Luft- und Raumfahrt (DLR) Remote Sensing Technology Institute (IMF)
- Science [&] Technology AS (ST)
- Technische Universität Dresden (TUDr)
- University College London (UCL/MSSL)
- University of Leeds, School of Earth and Environment (UL)

 antarctic ice sheet cci	Antarctic_Ice_Sheet_cci+ End-to-end Uncertainty Budget (E3UB)	Reference : ST-UL-ESA-AISCCI+-E3UB-001 Version : 1.0 page Date : 22 May 2020 2/20
---	--	---

Signatures page

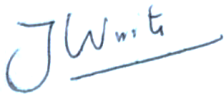


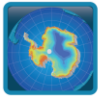
Prepared by	Jan Wuite Lead Author, ENVEO		Date: 20 May 2020
Issued by	Daniele Fantin, Project Manager, ST		Date: 22 May 2020
Checked by	Andrew Shepherd Science Leader, UL		Date: 22 May 2020
Approved by	Marcus Engdahl ESA Technical Officer		Date:

Table of Contents

Change Log	4
Acronyms and Abbreviations	5
1 Introduction	6
1.1 Purpose and Scope	6
1.2 Document Structure	6
1.3 Applicable and Reference Documents.....	6
2 End-to-end Uncertainty Budget for SEC.....	7
2.1 Introduction	7
2.2 Sources of error	7
2.2.1 Instrument, orbit, and position errors.....	7
2.2.2 RA penetration into the firn	8
2.2.3 Range correction and retracking errors	8
2.2.4 Errors due to surface slope and topography.....	8
2.2.1 Data gaps and interpolation.....	13
2.2.2 Inter-satellite elevation bias	13
2.3 Methodology for determination of error and uncertainty	14
2.4 Error and uncertainty documentation	15
2.5 Guideline for using the product	15
2.6 References	15
3 End-to-end Uncertainty Budget for IV	17
3.1 Introduction	17
3.2 Sources of error.....	17
3.2.1 Tide Model Errors.....	17
3.2.2 Atmospheric Pressure Errors.....	17
3.3 Methodology for determination of error and uncertainty	17
3.4 Error and uncertainty documentation	19
3.5 Guideline for using the product	19
3.6 Round Robin	19
3.7 References	20

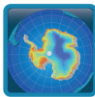


Change Log

Issue	Author	Affected Section	Change	Status
1.0	ENVEO	All	Document Creation	

Acronyms and Abbreviations

Acronyms	Explanation
AIS	Antarctic Ice Sheet
ATBD	Algorithm Theoretical Basis Document
CCI	Climate Change Initiative
CECR	Comprehensive Error Characterisation Report
DEM	Digital Elevation Model
DInSAR	Differential SAR Interferometry
DLR	Deutsches Zentrum für Luft- und Raumfahrt
DTU	Danmarks Tekniske Universitet
ECV	Essential Climate Variables
ENVEO	Environmental Earth Observation
ERS	European remote sensing satellite
IBE	Inverted Barometer Effect
IV	Ice Velocity
IVonIS	Ice Velocity on Ice Shelves
LRM	Low Resolution Mode
OCOG	Offset Centre of Gravity (OCOG) re-tracker
PUG	Product User Guide
RA	Radar Altimetry
RMSE	Root-Mean-Square Error
RR	Round Robin
S3MPC	Sentinel-3 Mission Performance Center
SAR	Synthetic Aperture Radar
SEC	Surface Elevation Change
SoW	Statement of Work
TCM	Tidal Correction Module
TFMR	Threshold First Maximum Retracking
TUDr	Technische Universität Dresden
UCL	University College London
UL	University of Leeds
UTC	Coordinated Universal Time

 antarctic ice sheet cci	Antarctic_Ice_Sheet_cci+ End-to-end Uncertainty Budget (E3UB)	Reference : ST-UL-ESA-AISCCI+-E3UB-001 Version : 1.0 page Date : 22 May 2020 6/20
--	--	---

1 Introduction

1.1 Purpose and Scope

This document contains the End-to-end Uncertainty Budget (E3UB) for the Antarctica_Ice_Sheet_cci (AIS_cci) project for CCI+ Phase 1, in accordance to contract and SoW [AD1 and AD2]. The central aim is to ascertain error characteristics that permit identification of climate change over natural variability. The E3UB describes the end to end errors of ECV improvements, proposed for CCI+, and builds on the Phase 2 Comprehensive Error Characterisation Report (CECR) document [RD1] of the 'Antarctic_Ice_Sheet_cci+ project.

The overall error and uncertainty budget for products with new technical developments will be provided or re-assessed and updated where needed, considering errors induced by new sensors, models, corrections, technical developments, and continued validation/inter-comparison efforts, including Round Robin outcomes. The document describes the best current understanding of the sources of errors, and uncertainties for the retrieval algorithms of the parameters: 'Surface Elevation Change (SEC)' and 'Ice Velocity (IV)'.

1.2 Document Structure

This document is structured into an introductory chapter followed by 2 chapters focussed on End-to-end Uncertainty Budget for the CCI+ parameters:

- Chapter 2: Surface Elevation Change (SEC)
- Chapter 3: Ice Velocity (IV)

1.3 Applicable and Reference Documents

Table 1.1: List of Applicable Documents

No	Doc. Id	Doc. Title	Date	Issue/ Revision/ Version
AD1	ESA/Contract No. 4000126813/18/I-NB, and its Appendix 2	CCI+ PHASE 1 - NEW R&D ON CCI ECVs, for Antarctic_Ice Sheet_cci	2019.09.30	
AD2	ESA-CCI-EOPS-PRGM-SOW-18-0118 Appendix 2 to contract.	Climate Change Initiative Extension (CCI+) Phase 1, New R&D on CCI ECVs Statement of Work	2018.05.31	Issue 1 Revision 6

Table 1.2: List of Reference Documents

No	Doc. Id	Doc. Title	Date	Issue/ Revision/ Version
RD1	ST-UL-ESA-AISCCI-CECR-001	CECR for the Antarctic_Ice_Sheet_cci project of ESA's Climate Change Initiative	2017.11.01	3.0
RD2	ST-UL-ESA-AISCCI+-ATBD-001	Antarctic_Ice_Sheet_cci+ Algorithm Theoretical Baseline Document (ATBD)	2020.04.14	1.0
RD3	ST-UL-ESA-AISCCI-PUG-001	Antarctic_Ice_Sheet_cci Product User Guide (PUG)	2018.06.26	1.4

Note: If not provided, the reference applies to the latest released Issue/Revision/Version

2 End-to-end Uncertainty Budget for SEC

2.1 Introduction

In this section the error sources, uncertainties, and methodology for characterisation of the errors of the derived surface elevation change from Ku-band radar altimetry are outlined. Satellite radar altimetry of ice sheets are characterized by a number of errors, some of which make their application for climate change measurements quite problematic, especially the problems of getting reliable data over the sloping coastal regions and outlet glaciers.

Table 2.1: Typical magnitude of errors in SEC.

Slope Correction	Corrects for slope-induced errors.	0 to 150
Retracking	Corrects for tracker lag.	-15 to 15
Tropospheric Refraction	Corrects for signal delay due to pressure variations and water vapour in the troposphere.	1.5 to 2.5
Ionospheric Refraction	Corrects for signal delay due to charged particles in the ionosphere.	.02 to .10
Tides (ocean and solid earth)	Removes earth and ocean dynamics.	-3 to 3
Ascending/descending bias	Biases between measurements on ascending and descending tracks	-2 to 2
Inter-satellite bias	Biases between measurements from different satellites	-2 to 3.5
Backscatter correction	Correction for dependence of elevation changes on changes in waveform parameters to correct variations in backscattering depth	± 1.5 to $\pm 3^*$

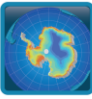
** Represents correction of elevation changes for the points of time series over grid cell. Range of correction depends on the correction method and applied retracking correction.*

2.2 Sources of error

The errors may be classified in a number of parameter groups, as outlined in the following subsections.

2.2.1 Instrument, orbit, and position errors

Pointing errors in pulse-limited RA is usually not an issue, as is the UTC timing of the satellite transmit and receive times, compared to the size of the radar footprint on the ground. Satellite orbit height errors for best post-processed orbits are typically 2-5 cm, and are, therefore, also not a major limitation issue in generating the RA essential climate variables (ECV). For the stability of the orbit and range measurement, the applications over ice sheets can benefit from the significant efforts made in calibrating and validating RA over oceans. A long-term stability at the cm-level has been demonstrated by several investigators in US and Europe across the ERS, Envisat and TOPEX missions (Faugere, 2007).

 antarctic ice sheet cci	Antarctic_Ice_Sheet_cci+ End-to-end Uncertainty Budget (E3UB)	Reference : ST-UL-ESA-AISCCI+-E3UB-001 Version : 1.0 page Date : 22 May 2020 8/20
--	--	---

2.2.2 RA penetration into the firn

Radar penetration at Ku-band into the firn is a major limitation in RA, with volume scattering down to several meter depth dominating the long tail of the altimeter waveform. The location of the leading edge will be a function of the snow density distribution, and especially the presence of ice lenses in the snowpack (ice lenses form regularly in the intermediate percolation zone of the ice sheet, in connection with the yearly thaw-refreeze cycle). Ice lenses and buried sastrugi structures are suspected to be major sources of bias frequently seen between ascending and descending orbits e.g. see Wingham (2006) or Khvorostovsky (2012). The effect of penetration depth on the measured RA elevations is also dependent on the retracking method and thresholds chosen. Static penetration biases will cancel out during repeated SEC measurements, and time variant biases can be removed by performing a backscatter correction (Wingham et al., 1998).

2.2.3 Range correction and retracking errors

The retracking and slope corrections are the dominant error source in ice sheet RA; geophysical corrections for ionospheric and atmospheric path delays are the source of additional errors, but are reasonably well understood and quantified from ocean RA. Choice of a robust retracker such as OCOG or TFMR is necessary for SEC estimation, as measurement density and precision over the whole ice sheet is more important than overall accuracy of measuring the snow-air interface. A trivial - but important - issue in RA is the use of a consistent reference system: TOPEX/Poseidon data do not refer to the same ellipsoid as the ERS/Envisat data. The difference of these systems is around 70 cm.

2.2.4 Errors due to surface slope and topography

The varying Antarctic topography (Figure 2.1) within the footprint of RA gives complicated return signal waveforms, and assigning the effective reflection point on the surface from the leading edge of the altimetric radar return waveform shape can be error prone and ambiguous, unless the radar instrument is especially designed for such surfaces (as in CryoSat-2's SARin mode). The spherical wave front of the pulse-limited radar pulse (used in ERS, ENVISAT and CryoSat-2's LRM mode) will – within the beam width of the radar pulse – have a first return from the nearest topography which can be significantly off (several km) from the satellite position on the ground. More recent missions such as Sentinel-3A, and 3-B use a delay-doppler (SAR) technique which delivers a 4-fold improvement in along track resolution (to ~300m) but its first return may be located up to 8km across track. Only CryoSat-2 is able to use interferometric techniques to locate the surface reflection in the across-track plane.

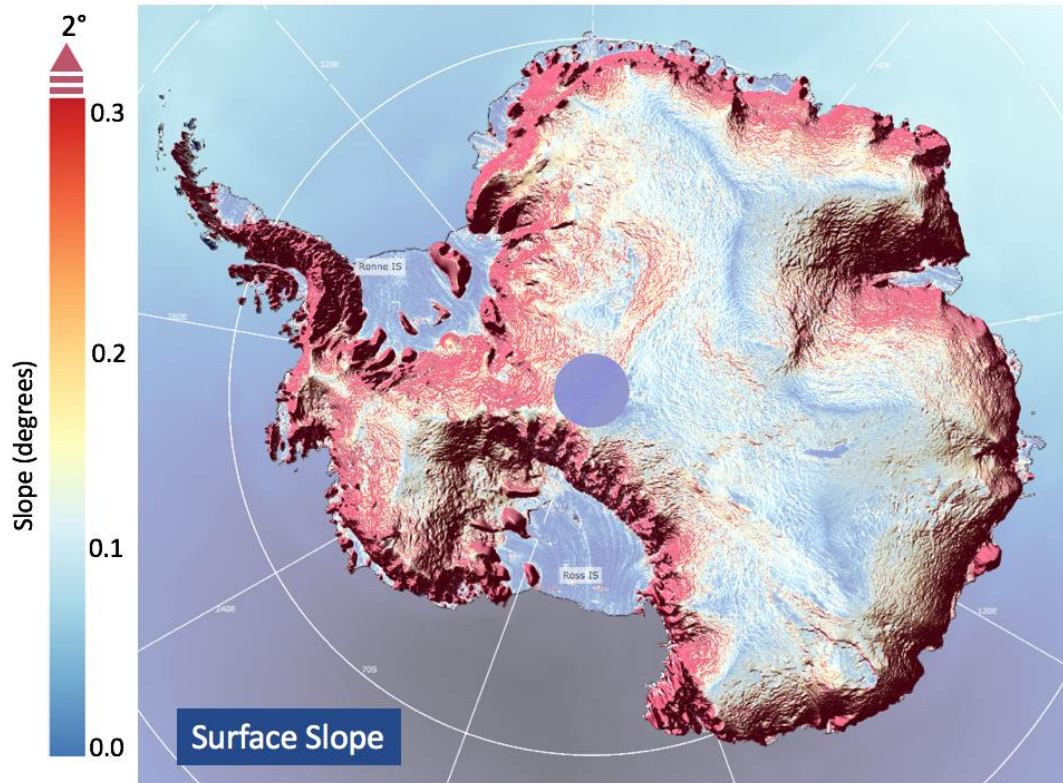
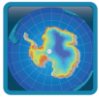


Figure 2.1: Surface Slope and Topographic Variability over Antarctica (Slope derived from CryoSat DEM, Slater, 2018)

Several methods for dealing with the problem of slope correction (for non-interferometric RA modes), have been proposed, e.g. Zwally (2015) or Brenner (1983), using either a correction for the off-nadir return assuming a linear sloping surface (keeping the ground reflection point at the satellite location), or relocating the orbit ground reflection point to the point of closest proximity using a DEM (moving the reflection point coordinates, and thus generating a “wiggly” non-equidistant trace of satellite reflection points instead of the regular satellite ground track). For a general review see Bamber, 1994. The spatial accuracy and resolution of the DEM, the time difference between the DEM and the measurement time, and relocation algorithm all effect the effectiveness of the slope correction. These are likely to improve over time and reduce the slope induced error.

Laser altimetry from ICESat and ICESat-2 does not have this limitation, due to the much narrower footprint (~70m, ~17m respectively), but data are only available over cloud free areas during the period of 2003-2009 (ICESat) and from Oct 2018 (ICESat-2), and will in the CCI+ project only be used for SEC validation.

RA measurement precision is of primary importance for derivation of SEC, and the effect of slope on the precision can be measured by crossover analysis. For pulse limited RA (ERS, ENVISAT, CryoSat-2 LRM), Schröder et al. (2019) showed that the precision of RA measurements decreases with increasing surface slope (Figure 2.2), but the decrease can be mitigated with improvements in slope correction and by optimised retracking.

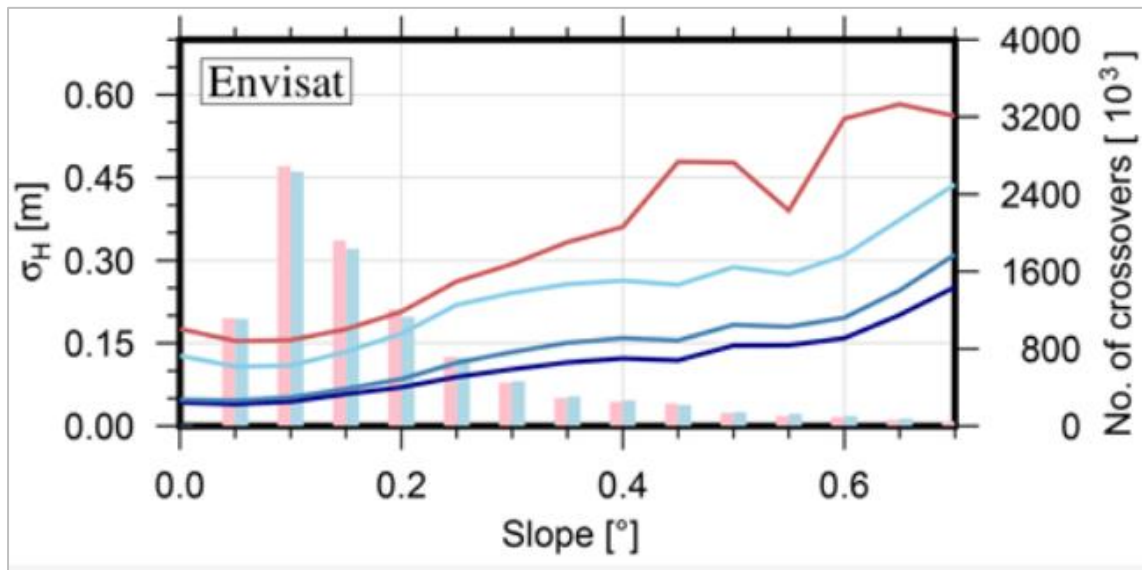
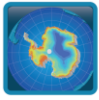


Figure 2.2: Precision of Envisat Measurements binned against slope (Schröder et al., (2019)). The different curves correspond to different slope corrections and retracker thresholds.

Sentinel-3A, and 3-B's slope dependent SAR measurement precision over Antarctica has also been measured by McMillan et al. (2019) and by the S3 Mission Performance Center (S3MPC) (Figure 2.3), however the final performance of S3 over the higher slope regions is being rapidly improved with frequent baseline releases and will not be fully determined until a dedicated optimised full land ice reprocessing of the missions is performed in late 2020.

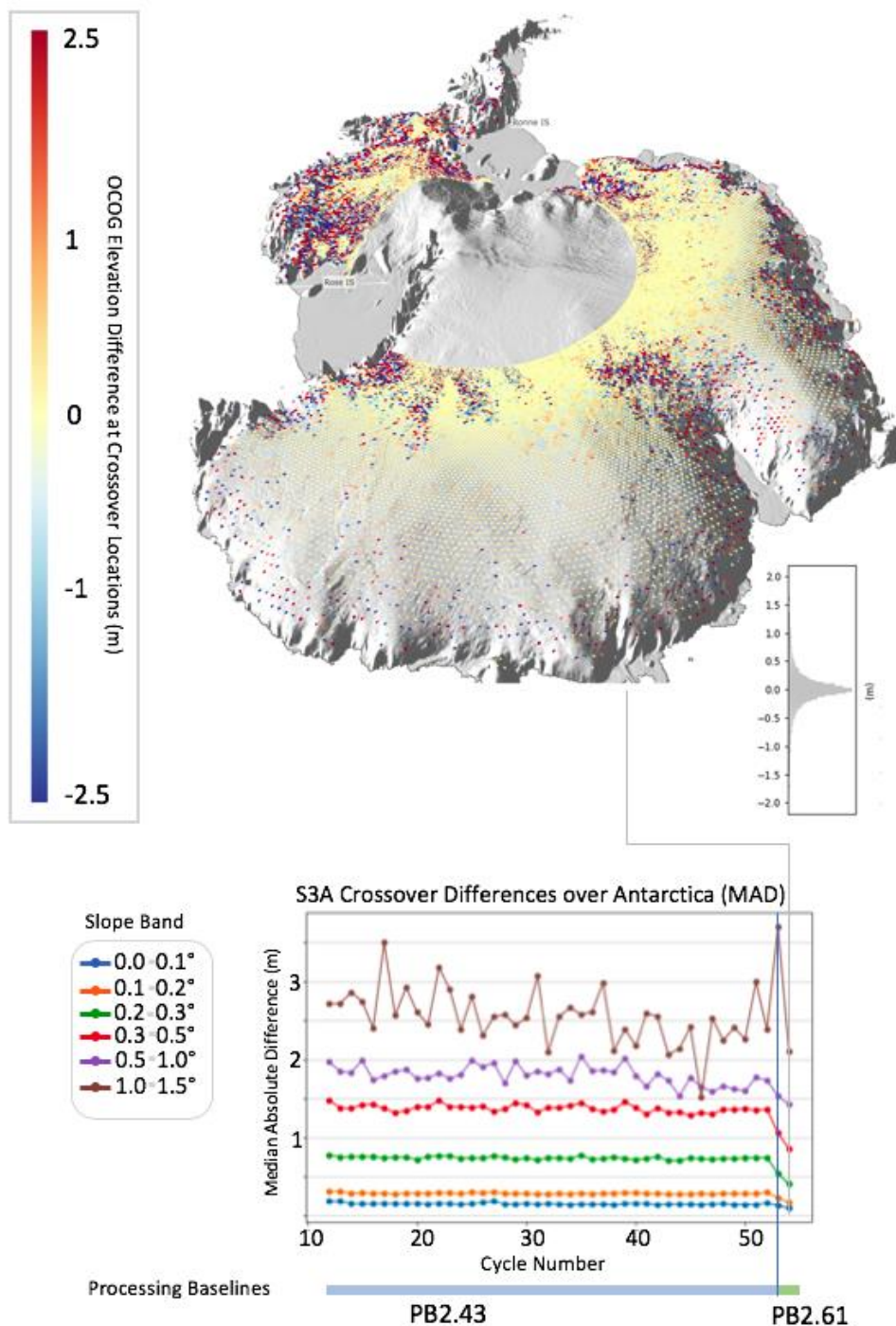
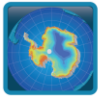


Figure 2.3: Precision of S3-A (OCOg retracker) for different bands of slope, showing improvements made in recent ESA processing baselines.



For CryoSat-2 in SARin mode over the Antarctic margins, a primary source of error is phase wrapping, and an incorrect detection of phase wrap can introduce errors of tens of meters. Phase ambiguity is currently detected (Figure 2.4) in the ESA products (baseline-D) but not corrected for.

The effect of slope and retracker type on CryoSat-2 SARin mode RA measurement precision over the Antarctic margins (a region of high slope and complex terrain) was also estimated by Schröder et al. (2019) in Figure 2.5. Although the slope-induced RA error can be very large, the effect on surface elevation change (SEC) is only a second order effect.

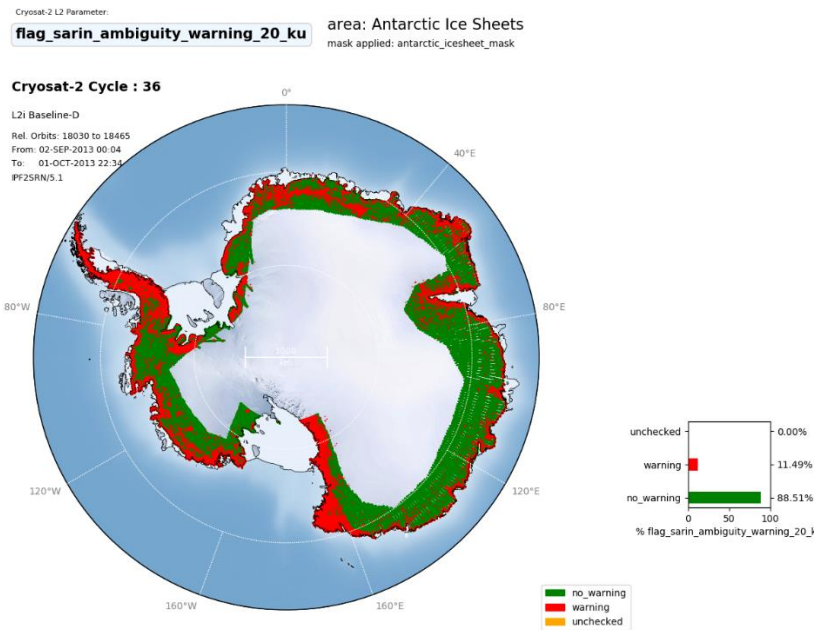


Figure 2.4: CryoSat-2 Phase Ambiguity Warning Flag

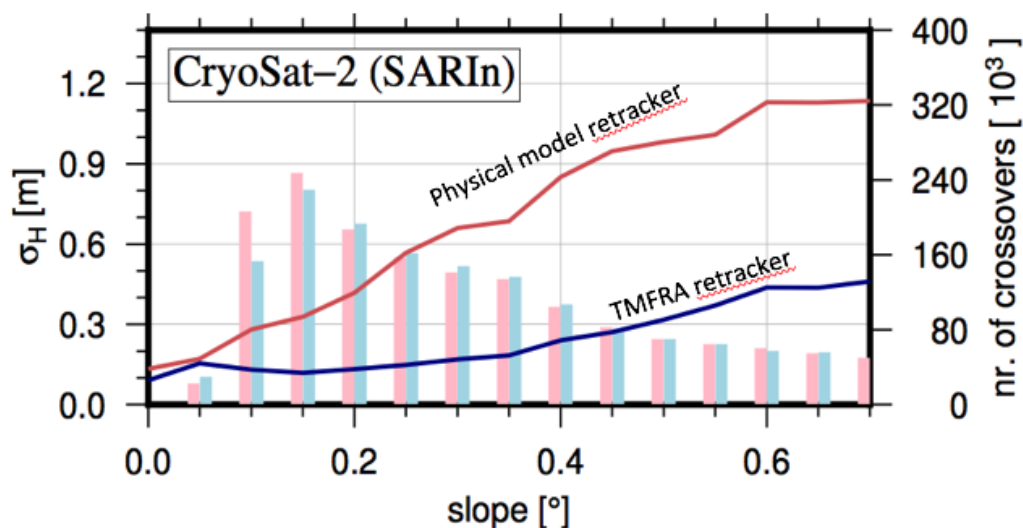


Figure 2.5: Precision of CryoSat-2 Measurements binned against slope (Schröder et al., (2019)).

2.2.1 Data gaps and interpolation

For estimation of the ECV product at 5 or 10 km resolution, RA measurements will leave many gaps (see Figure 2.6) due to the orbital pattern (especially for mission phases with a repeat cycle of ~ 30 days) and measurement failure (due to loss of track, low echo power, or complex waveforms that are difficult to retrack). The interpolation errors across these gaps will be determined by the covariance function of the satellite heights relative to a reference DEM, and the associated error covariance function of the grid values. To determine SEC from interpolated values at pixels away from repeated tracks is a challenge, and error estimates for this interpolation process will be based on repeat airborne laser validation data, where possible, and ICESat-2. When estimated errors become excessive, no SEC ECV value will be produced. This will likely be the case for most ice sheet areas of surface slopes of more than 1° (as shown in Figure 2.3)

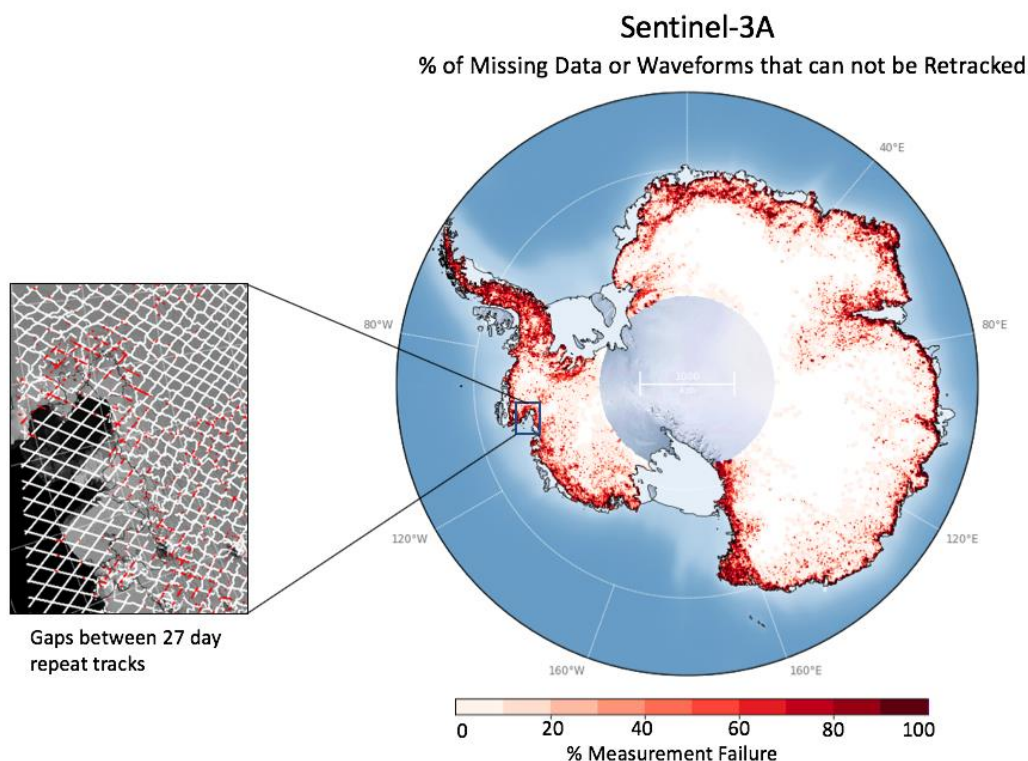


Figure 2.6: Typical Data Gaps and Measurement Failure for a 27-day Repeat Cycle of Sentinel-3A

2.2.2 Inter-satellite elevation bias

A full 27yr time series of elevations includes data from up to six RA missions, which must be co-registered to produce one continuous time series. Envisat is taken as the reference mission and its data is deemed to have no biases. Data from each other satellite is biased by a constant for that satellite over each grid cell. The biases between each temporally-overlapping pair of satellites are derived separately and combined later. For each overlapping pair of timeseries, the overlapping ends are modelled using least-squares regression to a seasonal cycle imposed on a linear gradient. The fitted model in each case is used to calculate elevation change in every month over a common two-year period, and the bias is taken as the median of the difference in the two elevation changes in this common period. This method can be adapted to calculate biases in areas larger than one pixel, e.g. by averaging all pixels in a drainage basin. The error due to the biasing is the root sum square of the 1-sigma uncertainties in the modelled differences between each overlapping pair.

2.3 Methodology for determination of error and uncertainty

Estimation of surface elevation errors are a propagation of errors of the individual measured RA heights, including the estimated interpolation error from optimal estimation using the residual covariance functions, combined with the errors of the estimated geophysical corrections. However, because many of these errors are correlated between epochs, the error estimates of surface elevation cannot readily be converted to errors in surface elevation change. Therefore, SEC 5km dh/dt errors using the plane fit solution (McMillan, 2014) are calculated from the 1-sigma uncertainty of the SEC trend (Figure 2.7). Errors in elevation time series are calculated using the root mean square of the departure from the modelled trend.

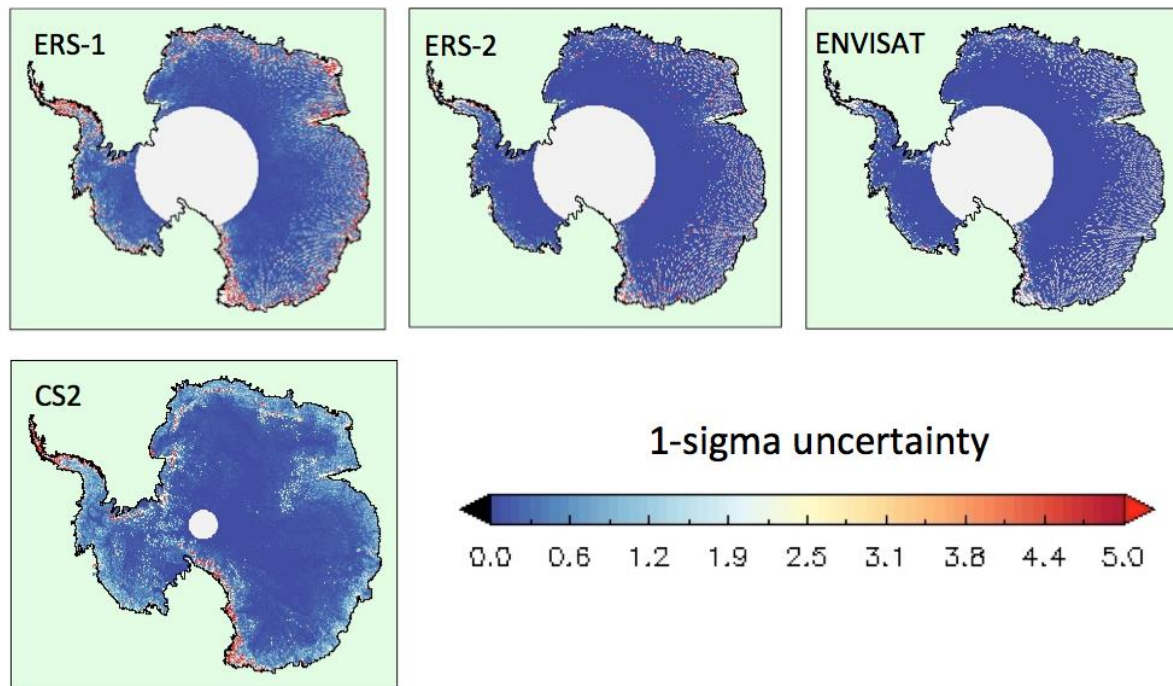
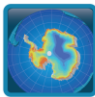


Figure 2.7: 1-sigma uncertainty of SEC dh/dt

Basin-wide elevation rate uncertainties are determined from the root sum square of the 1-sigma uncertainties, which are computed from all model solutions within each drainage basin, and from the biasing process. These uncertainties depend upon the distribution of elevation measurements accumulated within each grid cell and provide a measure of the extent to which our prescribed model of linear elevation change through time fits these observations. In consequence, they account for both departures from the prescribed model and for measurement errors which decorrelate within the sampling period, which is nominally 30 days. This statistical measure does not formally account for all sources of uncertainty, but will include factors such as radar speckle, errors in satellite location, retracker imprecision and unmodelled atmospheric attenuation (Wingham et al., 1998). When the spatial covariance of these error terms is assessed (Wingham et al., 1998), the variability is observed to decorrelate rapidly with increasing separation, in contrast to the covariance of the measured elevation rates themselves which remain relatively high. We interpret this to indicate that, at the scale of glaciological basins, these error terms alone do not adequately describe the certainty of estimates of mass imbalance. Specifically, the presence of signals, other than those of long-term imbalance, may introduce additional elevation rates over the observation period and must also be considered. These include snowfall variability and changes in snowpack characteristics.

ICESat, ICESat-2 and airborne laser data will be used as primary external data to evaluate the RA SEC, especially in the marginal zones and glacier systems where a long time history of airborne SEC is available.

 antarctic ice sheet cci	Antarctic_Ice_Sheet_cci+ End-to-end Uncertainty Budget (E3UB)	Reference : ST-UL-ESA-AISCCI+-E3UB-001 Version : 1.0 page Date : 22 May 2020 15/20
--	--	--

In the Antarctic CCI round robin experiment, the standard deviation of the differences between IceBridge and CCI Plane Fit SEC was 24.5cm/yr.

Further indications of systematic errors will come from comparisons of SEC across the different RA missions, ERS-1, ERS-2, Envisat, CryoSat-2 and Sentinel-3. The estimation of orbit biases between different methods will as a first approximation be done by comparison of ranges over marine areas, where mean sea level models combined with tidal models should in most cases be able to determine inter-mission orbit biases at the 10 cm level. It should be noted, however, that only spatially-invariant offsets mentioned in the footnotes to Table 2.1 can be found by comparison of ranges over marine areas. The inter-mission biases over land are spatially-variant, and improved estimation schemes have been discussed in Johannessen (2005) and Zwally (2005).

2.4 Error and uncertainty documentation

The overall errors in the SEC product will be a function of primarily the surface slope and the glaciological facies of the ice sheet regions (i.e., depending on bare ice, soaked, percolation or dry-snow zones). The overall accuracy of the products are difficult to quantify exactly prior to final ECV production phase, but error estimates across the ice sheet of 1-2 cm/yr seems realistic. This will, however, not apply to the ice sheet margin areas, where localized ice streams and glaciers will have much larger expected errors, or data be absent due to excessive surface slopes.

2.5 Guideline for using the product

The gridded ECV product for SEC in the Ice_Sheets_cci+ project will for the user provide both surface elevation change and estimated errors. The gridded representation of data will ensure that users have a product which is as close as possible for direct use, either as boundary/ground truth values for ice sheet modelling, media and outreach use, and – to some degree – for merging with other sensor change data (notably GRACE, IceSat-2 and other future ice change missions). Especially for joint estimations with GRACE the gridded representation of the ECV products mean that spatial averaging to recover SEC at a spectral resolution corresponding to GRACE is readily possible, even for non-specialists. The only drawback of the gridded representation at the given 5km resolution is the lack of resolution over narrow outlet glaciers, which typically show the largest changes.

2.6 References

- Bamber, J.: Ice Sheet Altimeter Processing Scheme. Int. J. Remote Sensing, vol. 15, 925-938, 1994.
- Brenner, A.C., R.A. Bindshadler, R.H. Thomas, H.J. Zwally: Slope-Induced Errors in Radar Altimetry Over Continental Ice Sheets, Journal of Geophysical Res., Vol. 88, 1983.
- Faugere, Y, J Dorandeu, F Lefevre, N Picot and P Femenias: Envisat Ocean Altimetry Performance Assessment and Cross-calibration, Proceedings of the Montreux Envisat Symposium, 2007
- Forsberg, R, L Sørensen, J Levinsen, J Nilsson: Mass loss of Greenland from from GRACE, CryoSat and ICESat. ESA CryoSat Symposium CD-proceedings, March 2013.
- Johannessen O M, K Khvorostovsky, M Miles, L Bobylev: Recent Ice-Sheet Growth in the Interior of Greenland. Science, Vol. 310 no. 5750 pp. 1013-1016, doi: 10.1126/science.1115356, 2005.
- Khvorostovsky K,: Merging and analysis of elevation time series over Greenland ice sheet from satellite radar altimetry. IEEE Trans. Geosc., Remote Sens., vol., 50, 1, pp. 23-36, 2012.
- Lacroix P., B. Legrésy, F. Rémy, F. Blarel, G. Picard, and L. Brucker, :Rapid change of snow surface properties at Vostok, East Antarctica, revealed by altimetry and radiometry, Remote Sens. Environ., vol. 133, no. 12, pp. 2633-2641, 2009.
- McMillan M., Muir A., Shepherd A., Escola R., Roca M., Aublanc J, Thibaut P., Restano M., Ambrozio A., Beneviste J. : Sentinel-3 Delay-Doppler altimetry over Antarctica, Cryosphere 2019.
- Jan Wuite, et al., End-to-end Uncertainty Budget (E3UB) for the Antarctic_Ice_Sheet_cci+ project of ESA's Climate Change Initiative, version 1.0 (2015).

- Schutz B. E., H. J. Zwally, C. A. Shuman, D. Hancock, and J. P. DiMarzio: Overview of the ICESat Mission. GRL, VOL. 32, L21S01, doi:10.1029/2005GL024009, 2005
- Shepherd, A. and Wingham, D.: Recent sea-level contributions of the Antarctic and Greenland ice sheets: Science, v. 315, p. 1529-1532, 2007.
- Shepherd, A. et al., Algorithm Theoretical Basis Document (ATBD) for the Antarctic Ice Sheet CCI project of ESA's Climate Change Initiative, version 2.1 (2017).
- Schröder, L., Horwath, M., Dietrich, R., Helm, V., Van Den Broeke, M. R., & Ligtenberg, S. R. (2019). Four decades of Antarctic surface elevation changes from multi-mission satellite altimetry. The Cryosphere, 13(2), 427-449.
- Sørensen, L.S., Simonsen, S.B., Nielsen, K., Lucas-Picher, P., Spada, G., Adalgeirsdottir, G., Forsberg, R., and Hvidberg, C.S.: Mass balance of the Greenland ice sheet (2003-2008) from ICESat data - the impact of interpolation, sampling and firn density. Cryosphere, v. 5, p. 173-186, 2011.
- Wingham D J, A Shepherd, A Muir, G.J Marshall: Mass balance of the Antarctic ice sheet. Phil. Trans. R. Soc vol. 364 no. 1844 1627-1635, doi: 10.1098/rsta.2006.1792, 2006.
- Vignudelli, S, A. G. Kostianoy, P. Cipollini, J. Benveniste (editors): Coastal Altimetry, Springer-Verlag, doi:10.1007/978-3-642-12769-0, 2011.
- Zwally, H J, M B Giovinetto, J Li, H G Cornejo, M A Beckley, A C Brenner, Jack L. Saba, Donghui Y: Mass changes of the Greenland and Antarctic ice sheets and shelves and contributions to sea-level rise: 1992–2002. Journal of Glaciology, Vol. 51, No. 175, 2005.

3 End-to-end Uncertainty Budget for IV

3.1 Introduction

The main upgrade of the ice velocity (IV) processing chain introduced in this cycle of the project is the development of a tidal correction module (TCM) to correct ice velocity for tidally induced vertical motion on floating ice (e.g. ice shelves, glacier tongues). The error characterisation of the processing chain developed in the first two CCI phases is documented in [RD1] and is not discussed in this document. The TCM processing chain being developed in the CCI+ project is described in [RD2].

3.2 Sources of error

Errors in the tide correction affect only the range component of velocity and stem primarily from errors in the tidal estimates and errors in the surface pressure model used to correct the non-steady (vertical) components of ice shelf motion. A preliminary performance test, described in [RD2], shows a clear reduction in the variance of ice velocity from Sentinel-1 on Larsen C ice shelf when applying the TCM.

3.2.1 Tide Model Errors

Ocean tides around Antarctica are often poorly constrained. Studies have shown that in some Antarctic regions comparisons between in situ data and model results show ocean tide model errors of 0.1 m for one or more tidal constituents, which is substantially above the error of tide models in the deep open ocean (King et al., 2011). The TCM under development in Antarctic Ice Sheet CCI+ utilizes the CATS2008 tide model developed by Padman et al. (2002, 2008) and provided on a 4km grid by the U.S. Antarctic Program Data Center (USAP-DC) (Howard et al., 2019). In a study by McMillan et al. (2011) tide predictions from three models, including CATS2008, were evaluated with satellite based InSAR measurements from ERS-1/2 in the Amundsen Sea. All selected models performed comparably well with a root-mean-square-error (RMSE) in the order of ~9-10 cm. It was concluded that, based on this, tide model inaccuracies may introduce an error of 22 m/yr (6 cm/d) in the range component of the velocity. In the Weddell Sea, King et al (2011) did an intercomparison of tide models with available in-situ GPS data and found slightly lower values for CATS2008a with root-sum-square errors of 7–8 cm.

3.2.2 Atmospheric Pressure Errors

In addition to tides, atmospheric forcing causes vertical displacements of sea surface height, referred to as the Inverted Barometric Effect (IBE), which may reach up to ~40 cm and introduces another source of vertical ice shelf motion (Padman et al., 2003). The IBE is accounted for in the TCM using an atmospheric pressure model (European Centre for Medium-Range Weather Forecasts (ECMWF) ERA-5 reanalysis). IBE is generally smaller than the daily mean tide levels but larger than the typical tide model error, which is in the order of 10 cm. Therefore, IBE is the second largest contribution to the changing sea surface height (Padman et al., 2003). Limited independent observations by King (2003) indicated a 1.05 hPa standard deviation of the model predictions which can be used as an estimate of the error associated with model estimates of atmospheric pressure, yielding errors of 1-2 cm in the vertical correction.

3.3 Methodology for determination of error and uncertainty

The uncertainty budget for the magnitude of the IV in the current framework is dependent on the tide model error, atmospheric pressure error and the uncorrected IV error. The uncertainty is reduced by redundant observations which are combined in a least-squares sense. The least-squares estimation allows for a comprehensive weighting of the displacement observations and can subsequently provide error estimates of the projected displacement vectors. The inclusion of the tide model affects the range components' magnitude



and uncertainty. To that end, an additional weighting is introduced to the range component observation to account for the tidal model uncertainty. The weighting of range displacements is reduced with a factor f_{tide} over the ice shelf due an increased uncertainty with respect to azimuth displacement observations. The tide model is absent over grounded ice, such that no tide-related weighting is applied here. The relative contribution of f_{tide} is modelled with the weighting mask, w_{mask} , from 3.3.1 from the ATBD [RD2] via:

$$w_{tot,i} = w_{uncor,i} * (1 - w_{mask,i} * f_{tide,i}), \quad \text{Equation 3.1}$$

where $w_{tot,i}$ is the least-squares total weight for a tide corrected range displacement observation i , and $w_{uncor,i}$ is the normalised weight for an uncorrected range displacement observation i . $w_{mask,i}$ is 0 over land and increases to unity when crossing the grounding line. A $f_{tide,i}$ of 0.1 yields reasonable results. The least-squares system remains the same except for the adjusted weighting vector W .

$$\hat{x} = (A^T W A)^{-1} A^T W y, \quad \text{Equation 3.2}$$

where \hat{x} is a vector containing the least-squares estimated ground displacements. A is the design matrix, projecting the azimuth and range displacements to ground displacements and y is a vector containing the range and azimuth displacements. Residuals r can be computed via:

$$r = y - A\hat{x}. \quad \text{Equation 3.3}$$

The residuals can be used to compute the variance of the observations with respect to the model:

$$\sigma_y^2 = \frac{r^T W r}{N-1}, \quad \text{Equation 3.4}$$

where N is the number of observations. The variance-covariance, $Q_{\hat{x}\hat{x}}$, of the estimated parameters can then be derived by propagation via:

$$Q_{\hat{x}\hat{x}} = \sigma_y^2 (A^T W A)^{-1}, \quad \text{Equation 3.5}$$

where the variances of the ground displacements can be found on the main diagonal of $Q_{\hat{x}\hat{x}}$. Figure 3.1 shows an example of the standard deviations of the East-West and North-South component on Larsen C for February 2020.

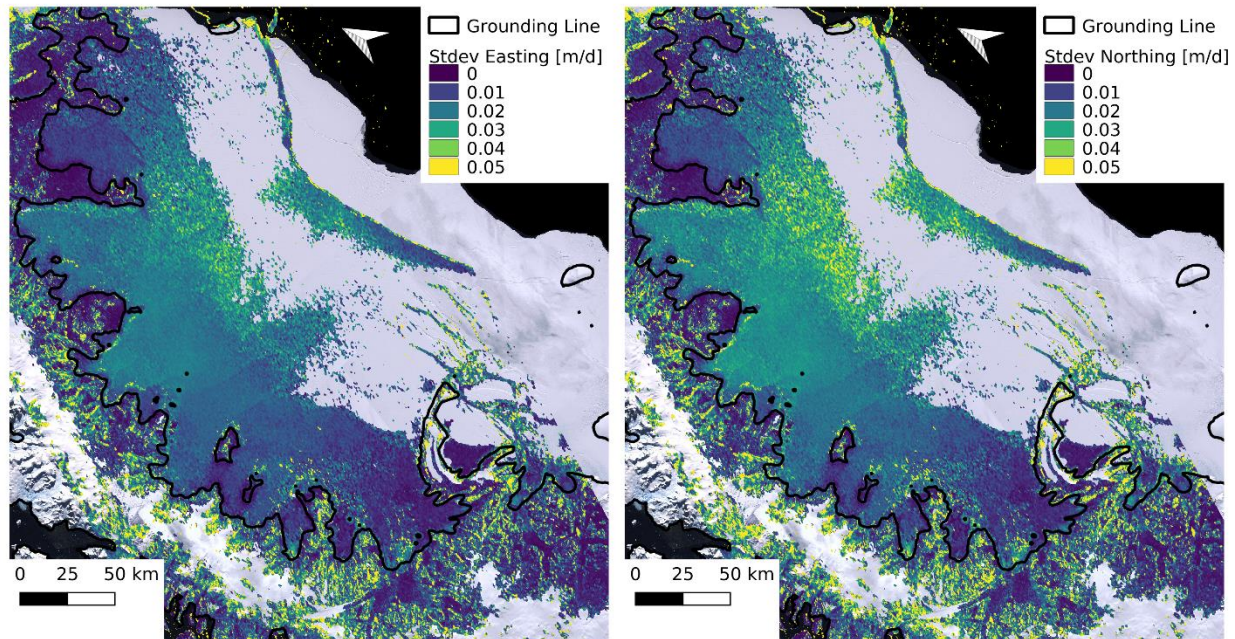


Figure 3.1: Standard deviations of the East-West and North-South component on Larsen C for Sentinel-1 derived ice velocity (track 38) for February 2020 (background: USGS LIMA Landsat mosaic).

3.4 Error and uncertainty documentation

Each generated map of a Cartesian velocity component is accompanied by its associated error standard deviation. The latter is also a map, in the same geometry as the associated measurement, providing a measure of uncertainty on a per-pixel basis.

3.5 Guideline for using the product

The IV product can be distributed as NetCDF or GeoTiff files following the conventions described in the Antarctic_Ice_Sheet_cci Product User Guide (PUG)(RD3). The estimated error standard deviations are provided in the same grid as the ice velocity estimates.

3.6 Round Robin

Within AIS CCI+ a round robin (RR) on ice velocity retrieval on ice shelves (IVonIS) from Sentinel-1 SAR data has been performed in which three partners of the project participated (for details see Annex to RD2). The participants were asked to process approximately 1 month (or one full tidal cycle) of Sentinel-1 SAR data covering the Larsen C Ice Shelf in the Antarctic Peninsula and provide velocity maps for each repeat pair (in total 5) with and without tidal correction applied. The results were intercompared on a pixel-by-pixel level as well as with a reference map, compiled from longer-term averaged ice velocity (6-months) centred on the RR SAR acquisition dates. In addition, two tide models and surface pressure reanalysis data sets were intercompared using the RR data sets. The products from the participants clearly illustrate the efficacy of the tide corrections with mean differences with longer-term averaged ice velocity strongly reduced from 10/20+ cm/day to only 1-5 cm/day with an RMSE in the order of 10 cm/d. Based on the outcome the general approach outlined in RD2 is selected and implemented. Figure 3.2 serves as illustration of the improvement achieved by implementing the tide correction. Remaining deviations between the short term and reference map can form the basis for further improvement of existing tide models.

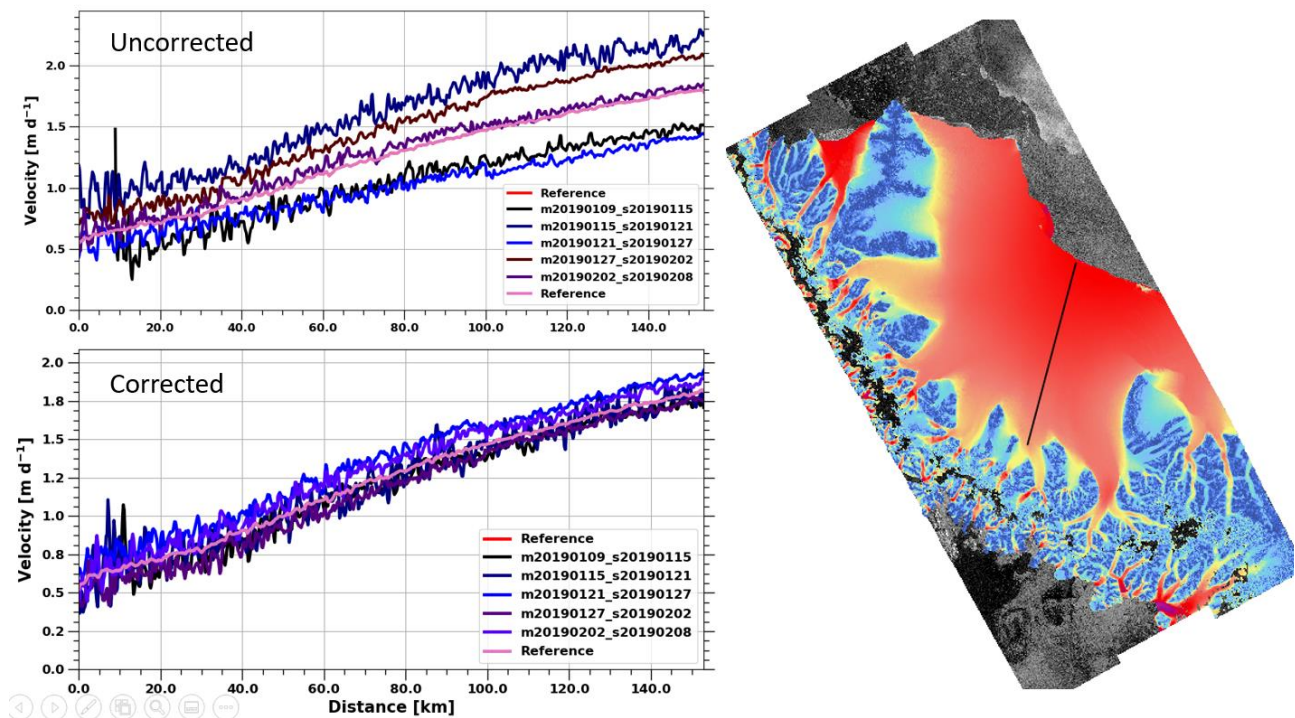


Figure 3.2: Ice velocity (magnitude) along a profile before (top) and after (bottom) tide correction. Location of the profile is indicated on the velocity map (right).

3.7 References

- King, J. C. (2003), Validation of ECMWF sea level pressure analyses over the Bellingshausen Sea, Antarctica, *Weather Forecast.*, 18(3), 536– 540.
- King, M. A. et al. (2011) 'Ocean tides in the Weddell Sea: New observations on the Filchner-Ronne and Larsen C ice shelves and model validation', *Journal of Geophysical Research*, 116(C6), p. C06006. doi: 10.1029/2011JC006949.
- McMillan, M. et al. (2011) 'Tide model accuracy in the Amundsen Sea, Antarctica, from radar interferometry observations of ice shelf motion', *Journal of Geophysical Research*, 116(C11), p. C11008. doi: 10.1029/2011JC007294.
- Padman, L., H. A. Fricker, R. Coleman, S. Howard, and S. Erofeeva (2002), A new tidal model for the Antarctic ice shelves and seas, *Ann. Glaciol.*, 34, 247-254. (doi:10.3189/172756402781817752)
- Padman, L. et al. (2003) 'Ice-shelf elevation changes due to atmospheric pressure variations', *Journal of Glaciology*, 49(167), pp. 521–526. doi: 10.3189/172756503781830386.
- Padman, L., L. Erofeeva, and H. A. Fricker (2008), Improving Antarctic tide models by assimilation of ICESat laser altimetry over ice shelves, *Geophys. Res. Lett.*, 35, L22504. (doi:10.1029/2008GL035592)